RESEARCH ARTICLE | APRIL 17 2023

Magnetization switching process by dual spin–orbit torque in interlayer exchange-coupled systems ⊘

Hiroto Masuda ✉ 🆔 ; Yuta Yamane 🆔 ; Takeshi Seki ✉ 🆔 ; Klaus Raab 🆔 ; Takaaki Dohi 🆔 ;
Rajkumar Modak 🆔 ; Ken-ichi Uchida 🆔 ; Jun'ichi Ieda 🆔 ; Mathias Kläui 🆔 ; Koki Takanashi 🆔

Check for updates

CrossMark

View
Online

Export
Citation

Magnetization switching process by dual spin–orbit torque in interlayer exchange-coupled systems

View Online   Export Citation   CrossMark

Hiroto Masuda,[1,2,a)] (iD) Yuta Yamane,[3,4] (iD) Takeshi Seki,[1,5,a)] (iD) Klaus Raab,[6] (iD) Takaaki Dohi,[6,7] (iD)
Rajkumar Modak,[5] (iD) Ken-ichi Uchida,[1,5] (iD) Jun'ichi Ieda,[8] (iD) Mathias Kläui,[6] (iD) and Koki Takanashi[1,8] (iD)

AFFILIATIONS

[1]Institute for Materials Research, Tohoku University, Sendai 980-8577, Japan
[2]Department of Materials Science, Graduate school of Engineering, Tohoku University, Sendai 980-8579, Japan
[3]Frontier Research Institute for Interdisciplinary Sciences, Tohoku University, Sendai 980-0845, Japan
[4]Research Institute of Electrical Communication, Tohoku University, Sendai 980-8577, Japan
[5]Research Center for Magnetic and Spintronic Materials, National Institute for Materials Science, Tsukuba 305-0047, Japan
[6]Institut für Physik, Johannes Gutenberg-Universität Mainz, Staudingerweg 7, 55128 Mainz, Germany
[7]Laboratory for Nanoelectronics and Spintronics, Research Institute of Electrical Communication, Tohoku University,
  Sendai 980-8577, Japan
[8]Advanced Science Research Center, Japan Atomic Energy Agency, Tokai 319-1195, Japan

[a)]Authors to whom correspondence should be addressed: hiroto.masuda.q5@dc.tohoku.ac.jp and takeshi.seki@tohoku.ac.jp

ABSTRACT

We report current-induced magnetization switching in Pt/Co/Ir/Co/Pt multilayers with different Ir layer thicknesses (t_{Ir}), where the perpendicularly magnetized Co layers are coupled ferromagnetically or antiferromagnetically through an interlayer exchange coupling and are sandwiched by the Pt spin Hall layers. The domain structures formed during switching vary depending on the magnetization alignment, i.e., a ferromagnetically coupled or antiferromagnetically coupled configuration. These results clarify the macroscopic picture of switching process for interlayer exchange-coupled systems. The local picture of the switching process is also examined by a numerical calculation based on a macrospin model, which reveals the switching dynamics triggered by dual spin–orbit torques for both antiferromagnetically and ferromagnetically coupled cases. The numerical calculation shows that the dual spin–orbit torques from the two Pt layers effectively act on the two Co layers not only for the antiferromagnetically coupled case but also for the ferromagnetically coupled one. Our findings deepen the understanding of the switching mechanism in a magnetic multilayer and provide an avenue to design spintronic devices with more efficient spin–orbit torque switching.

Published under an exclusive license by AIP Publishing. https://doi.org/10.1063/5.0140328

Antiferromagnetic materials garner attention[1–3] because of low magnetic susceptibility,[4] lack of magnetic stray field, and fast magnetization dynamics reaching the terahertz-order resonance frequency,[5–7] which are suitable to realize spintronic devices enabling ultrahigh density and ultrafast operation. The spin–orbit torque induced by the spin Hall effect is one of the techniques to electrically control antiferromagnetic structures as well as ferromagnetic structures.[8] For example, in a tri-layer system of nonmagnet/antiferromagnet/nonmagnet, where the nonmagnet with a large spin–orbit coupling shows the spin Hall effect allowing the conversion of a charge current into a spin current, the accumulated spin angular momentum at both the top and bottom interfaces are transferred to the antiferromagnetic structure. The spin–orbit torques then act on each sublattice of the magnetic moment, resulting in the switching of antiferromagnetic alignment. Electrical magnetization switching in a antiferromagnetic structure was first reported for bulk antiferromagnets.[9–16] However, the complicated domain structures of bulk antiferromagnets[10,11,17] are unfavorable for efficient spin–orbit torque switching. The uncontrollable exchange coupling strength also hinders a systematic investigation. Instead of bulk antiferromagnets, a synthetic antiferromagnet is focused on in

20 July 2023 08:58:17

Refs. 18–51. In a tri-layer system consisting of ferromagnet/nonmagnet/ferromagnet, magnetizations of top and bottom ferromagnetic layers couple with each other ferromagnetically or antiferromagnetically due to the interlayer exchange coupling.[52] The interlayer exchange coupling strength can be modulated by simply changing the layer thicknesses, enabling the systematic experiments of the spin–orbit torque switching in the coupled system. Current-induced magnetization switching in a synthetic antiferromagnet has been demonstrated with interlayer materials of Ta,[22,27,29,39,44] Ru,[21,25,26,41,46] and Ir.[42,48] The Ta interlayer shows both the spin Hall effect and the interlayer exchange coupling, but its interlayer exchange coupling strength is small ($\sim 0.01 \times 10^{-3}$ J m^{-2}, Ref. 53). On the other hand, Ru and Ir interlayers lead to a remarkable interlayer exchange coupling strength in wide thickness ranges, where the first peak values of antiferromagnetic coupling strength are larger than 5×10^{-3} J m^{-2};[40,53] however, they usually do not show a remarkable spin Hall effect. Instead, the spin–orbit torque switching is realized by setting an additional spin Hall layer adjacent to a synthetic antiferromagnet. Previous studies have eagerly investigated the spin–orbit torque switching in antiferromagnetically coupled systems. However, the switching behavior for the film with dual spin Hall layers is still unclear in the case of interlayer exchange-coupled films although there are several studies on the dual spin Hall layers for the single ferromagnetic layer cases.[54–58]

Here, we report the current-induced magnetization switching in the interlayer exchange-coupled Co/Ir/Co system sandwiched by the Pt layers. The switching processes for different magnetization alignments, i.e., ferromagnetically coupled or antiferromagnetically coupled

configuration, were investigated by changing Ir layer thickness (t_{Ir}) through the electrical measurement and the magnetic domain imaging. The local picture for the switching process triggered by the dual spin–orbit torque was also clarified for both antiferromagnetically and ferromagnetically coupled cases by the numerical calculation based on the macrospin model.

Thin films consisting of Pt (2 nm)/Co (0.65 nm)/Ir (t_{Ir} = 0.45, 0.50, 0.80, or 1.30 nm)/Co (0.9 nm)/Pt (2 nm) were deposited on a thermally oxidized Si substrate using magnetron sputtering at room temperature with a base pressure below 6.0×10^{-6} Pa. Ta was deposited as 1 nm thick buffer and capping layers before and after deposition of the Pt/Co/Ir/Co/Pt, respectively. We expected the interlayer exchange coupling in the Co/Ir/Co tri-layer and the perpendicular magnetic anisotropy induced by Pt layers on magnetizations in Co layers. Magnetization curves are shown in Figs. 1(a)–1(d), which were measured by the vibrating sample magnetometer at room temperature. At t_{Ir} = 0.45 nm, both the out-of-plane and the in-plane magnetization curves exhibited the remanent magnetization, indicating that the magnitude of perpendicular magnetic anisotropy is insufficient for achieving the fully perpendicularly magnetized state. This is possibly due to the non-perfect film growth of the top Co layer on the thin Ir layer. However, at $t_{Ir} \geq 0.50$ nm, the perpendicular magnetic anisotropy overcomes the out-of-plane demagnetizing field, resulting in the perpendicularly magnetized state. Low (large) remanent magnetization and large (small) saturation field at t_{Ir} = 0.50 and 1.30 nm (at t_{Ir} = 0.80 nm) indicate the antiferromagnetic coupling (ferromagnetic coupling) in the Co/Ir/Co structure, being consistent with our previous report.[49]
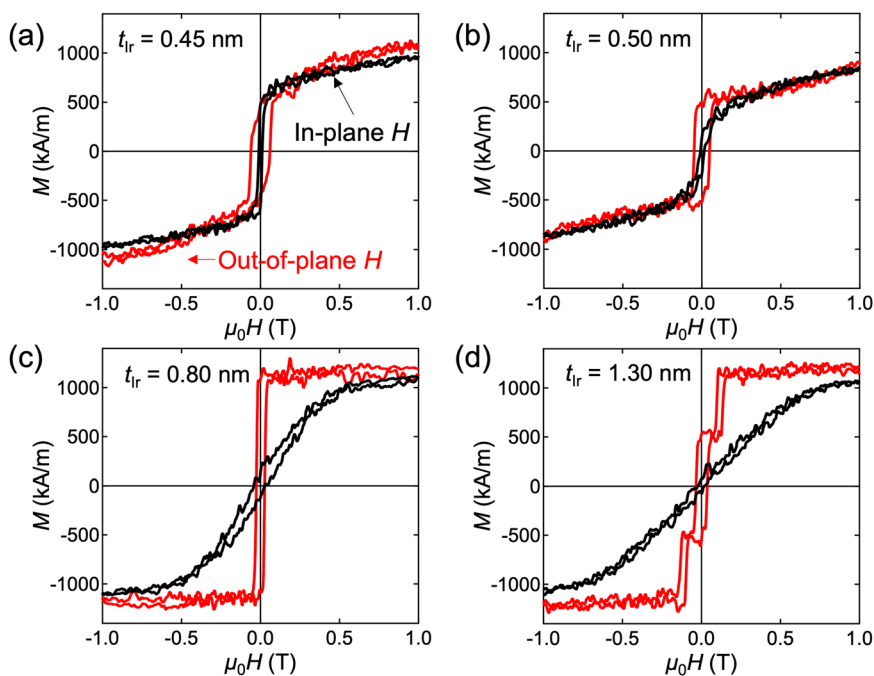

FIG. 1. Magnetization curves for Pt/Co/Ir (t_{Ir})/Co/Pt samples with (a) t_{Ir} = 0.45, (b) t_{Ir} = 0.50, (c) t_{Ir} = 0.80, and (d) t_{Ir} = 1.30 nm. Red and black curves were obtained by applying the out-of-plane magnetic field and the in-plane magnetic field, respectively.

For the current-induced magnetization switching measurement, thin films were patterned into Hall-bar-shaped devices with 5 μm wire width using photolithography and Ar-ion milling. Each device has the electrical contact pads of Cr (20 nm)/Au (200 nm) deposited by ion-beam sputtering. Figure 2(a) schematically illustrates the damping-like spin–orbit torque in the antiferromagnetically and the ferromagnetically coupled Pt/Co/Ir/Co/Pt structures with magnetization **m** for each Co layer. The application of a charge current with a current density j_c in the x direction induces the spin current density j_s in the z direction in Pt layers due to the spin Hall effect. The ratio of conversion is expressed as the spin Hall angle: $\theta_{SH} = (2e/\hbar) j_s/j_c$, where e and $\hbar$ denote the elementary charge and the Dirac's constant, respectively. The spin moments σ accumulate at the interfaces pointing in the $\pm y$ direction, generating the damping-like spin–orbit torque (τ_{DL}) proportional to $\mathbf{m} \times (\mathbf{m} \times \sigma)$.[59] The effective field of damping-like spin–orbit torque (B_{DL}) then works parallel to $\mathbf{m} \times \sigma$ on magnetizations. For the antiferromagnetically coupled system, B_{DL} acting on both top and bottom Co layers point in the $-x$ direction. On the other hand, for the case of the ferromagnetically coupled system, B_{DL} acts in the $-x$ direction for the top side and in the $+x$ direction for the bottom side. One may anticipate that B_{DL} for the top Co and B_{DL} for the bottom Co cancel out in the case that two Co layers are strongly coupled, which is regarded as the condition that dual spin–orbit torque with opposite signs simultaneously acts on the single ferromagnetic layer. As it will be shown, however, the ferromagnetically coupled system having a moderate coupling strength exhibits a different behavior from that of the single ferromagnetic layer.

The measurement setup for the four-probe method is depicted in Fig. 2(b). A DC charge current (I_{dc}) with pulse width of ∼100 ms was applied in the x direction using a Keithley 2400 DC source meter. The Hall resistance (R_{xy}) was detected by applying an AC charge current of 20 μA with a frequency of 9997 Hz using a lock-in amplifier SR830 after each application of I_{dc}. An external magnetic field of 80 mT was also applied simultaneously in the x direction to assist the magnetization switching. The values of R_{xy} as a function of I_{dc} for the devices with $t_{Ir} = 0.45$, 0.50, 0.80, and 1.30 nm are shown in Figs. 2(c)–2(f), respectively. The R_{xy}–I_{dc} curves with hysteresis were observed for all the samples, suggesting that magnetization switching is induced by the I_{dc} application. The R_{xy}–I_{dc} curves for $t_{Ir} = 0.45$ and 0.80 nm show the gradual change in R_{xy} with positive I_{dc} in the transition from a low resistance state to a high resistance state. Compared with these R_{xy}–I_{dc} curves, R_{xy} was sharply changed at I_{dc} ∼16.5 and −23.6 mA (12.6 and −17.4 mA) for the antiferromagnetically coupled sample with $t_{Ir} = 0.50$ nm (1.30 nm). The difference in R_{xy}–I_{dc} curves indicates that the switching process depends on the magnetization alignment via inter-layer exchange coupling. It is noted that the asymmetry in the positive and negative switching currents means that the observed R_{xy}–I_{dc} curves are minor loops. This is attributed to the domain-wall trapping at the intersected region between the channel and the branches of Hall-bar-shaped device which will be discussed in a later paragraph.

In order to understand the switching process in detail, the domain structures were visualized using a commercial Evico magnetics GmbH Kerr microscopy with an in-plane magnetic field coil. Figures 3(a)–3(d) display the domain structures under $\mu_0 H_x = 80$ mT, visualized after the application of I_{dc} for $t_{Ir} = 0.45$, 0.50, 0.80, and 1.30 nm, respectively. First, $I_{dc} > 22$ mA was applied in the $+x$ direction, which led to the saturated magnetic state. The images at $I_{dc} > 22$ mA were used as the background signal and subtracted from the obtained images. For all the
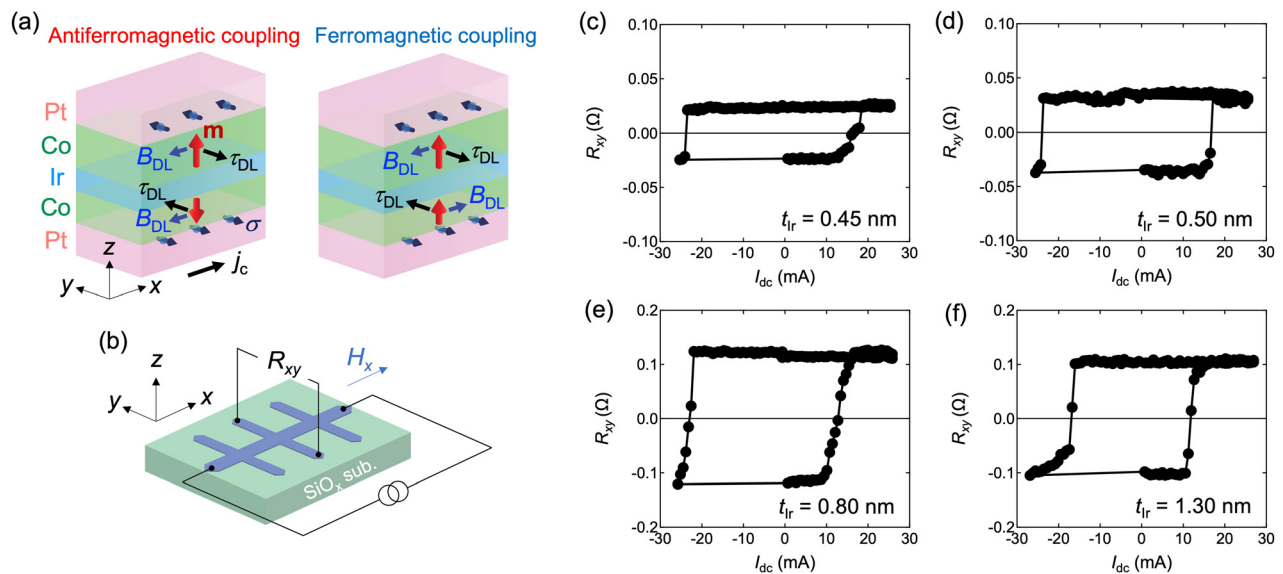

FIG. 2. Current-induced magnetization switching in Pt/Co/Ir/Co/Pt systems. (a) Schematic illustration of spin–orbit torque in the antiferromagnetically coupled and the ferromagnetically coupled Pt/Co/Ir/Co/Pt systems. A charge current with the current density (j_c) is applied in the x direction. The spin Hall effect in Pt layers induces the spin accumulation at the Pt/Co and Co/Pt interfaces, generating the damping-like spin–orbit torques (τ_{DL}) in top and bottom Co layers. **m**, σ, and B_{DL} denote the magnetization in the Co layer, the accumulated spin moments, and the effective field of damping-like spin–orbit torque, respectively. (b) Measurement setup of four-probe method under the application of magnetic field in the x direction (H_x) with the coordinate system. (c)–(f) R_{xy} as a function of a DC charge current under $\mu_0 H_x = 80$ mT for the devices with (c) $t_{Ir} = 0.45$, (d) $t_{Ir} = 0.50$, (e) $t_{Ir} = 0.80$, and (f) $t_{Ir} = 1.30$ nm.
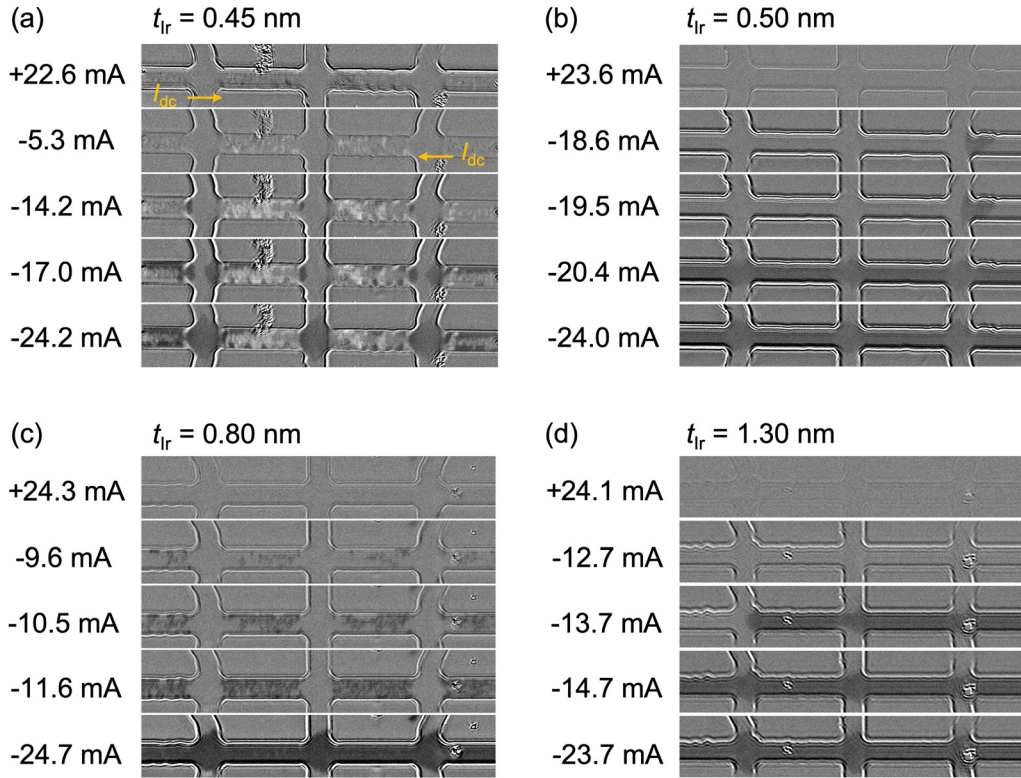
FIG. 3. Domain structures during current-induced magnetization switching observed by Kerr microscopy for Pt/Co/Ir (t_{Ir})/Co/Pt samples with (a) $t_{Ir} = 0.45$, (b) $t_{Ir} = 0.50$, (c) $t_{Ir} = 0.80$, and (d) $t_{Ir} = 1.30$ nm. Values of I_{dc} are shown in the left side of figures. $\mu_0 H_x = 80$ mT was applied during the measurements.

samples, the black and white contrast changes were observed with varying I_{dc}. For $t_{Ir} = 0.45$ nm, the complicated white regions were observed at $I_{dc} = -5.3$ mA. The black regions also appeared at $I_{dc} \leq -14$ mA. The complicated and intermixed contrasts for $t_{Ir} = 0.45$ nm are attributed to the existence of not only out-of-plane magnetized component but in-plane magnetized component as well, which is in agreement with the magnetization curves. For the antiferromagnetically coupled samples with $t_{Ir} = 0.50$ and 1.30 nm, the abrupt expansion of black region was observed, being consistent with the R_{xy}–I_{dc} curves showing the sharp change in R_{xy}. On the other hand, the ferromagnetically coupled sample with $t_{Ir} = 0.80$ nm showed a sparse nucleation at $I_{dc} = -9.6$ mA, and the switched region gradually increased with increasing $|I_{dc}|$. This is an apparent difference in the magnetic domain structures formed during the spin–orbit torque switching between the antiferromagnetic coupling case and the ferromagnetic coupling case. It is worth noting that the domain-wall trappings were observed in the intersected regions between the channel and the branches of Hall device for all the samples. This behavior is reminiscent of the magnetic ratchet effect found in the device with asymmetric configuration,[60] which would induce the asymmetric hysteresis in the minor loop as observed in Fig. 2. One may anticipate the formation of skyrmion bubbles in the Pt/Co/Ir structure,[61] but we did not observe it possibly due to the decrease in the interfacial Dzyaloshinskii–Moriya interaction[31] and the relatively large perpendicular magnetic anisotropy in the present Pt/Co/Ir/Co/Pt films.

Considering that the magnetization switching occurs through the nucleation of a reversed domain and the subsequent domain

expansion as visualized in Fig. 3, the nucleation of a reversed domain is triggered by the spin–orbit torque, and we may assume that the spin–orbit torque locally acts on the Co magnetization for some parts of the device. To understand the local picture of current-induced magnetization switching in Pt/Co/Ir/Co/Pt systems, we numerically simulated the spin–orbit torque switching dynamics. Let us consider the magnetic multilayer systems consisting of two coupled ferromagnetic layers, FM1 and FM2, with a common saturation magnetization (M_s) and thicknesses t_{m1} and t_{m2}, sandwiched by the spin Hall layers. The surface magnetic energy density (E) was assumed to be

$$E = J_{IEC}\mathbf{m}_1 \cdot \mathbf{m}_2 - K\left[t_{m1}\left(m_1^z\right)^2 + t_{m2}\left(m_2^z\right)^2\right]$$
$$- \mu_0 M_s \mathbf{h}_x \cdot (t_{m1}\mathbf{m}_1 + t_{m2}\mathbf{m}_2), \qquad (1)$$

where J_{IEC} is the interlayer exchange coupling strength, K is the perpendicular magnetic anisotropy constant, $\mathbf{m}_1$ ($\mathbf{m}_2$) is the unit vector representing the magnetic moment in FM1 (FM2) layer, and $\mathbf{h}_x$ is the external magnetic field in the x direction. Here, we assumed that $J_{IEC} > 0$ (< 0) for the antiferromagnetically (ferromagnetically) coupled case. The dynamics of $\mathbf{m}_\mu$ ($\mu = 1$ and 2) were described by the coupled Landau–Lifshitz–Gilbert equations as follows:

$$\frac{\partial \mathbf{m}_\mu}{\partial t} = -\gamma \mathbf{m}_\mu \times \mathbf{h}_\mu + \alpha \mathbf{m}_\mu \times \frac{\partial \mathbf{m}_\mu}{\partial t} - \gamma \mathbf{m}_\mu \times (\mathbf{m}_\mu \times \boldsymbol{\sigma}_\mu), \qquad (2)$$

where γ is the gyromagnetic ratio, and α is the damping constant. The effective magnetic fields $\mathbf{h}_\mu$ were defined by

20 July 2023 08:58:17

$$\mathbf{h}_\mu = -\frac{1}{\mu_0 M_s t_{m\mu}} \frac{\delta E}{\delta \mathbf{m}_\mu}, \tag{3}$$

and the spin–orbit torques were characterized by

$$\boldsymbol{\sigma}_\mu = \pm \frac{\hbar \theta_{SH}}{2e\mu_0 M_s t_{m\mu}} j_c \mathbf{y}, \tag{4}$$

where the upper (lower) sign corresponds to $\mu = 1$ (2). Figures 4(a) and 4(b) show the calculated switching dynamics for the antiferromagnetically and the ferromagnetically coupled systems, respectively, with parameters of $\mu_0 H_x = -10$ mT, $t_{m1} = 0.8$ nm, $t_{m2} = 0.5$ nm, $|J_{IEC}| = 1.5 \times 10^{-3}$ J m^{-2},[49] $K = 5.7 \times 10^5$ J m^{-3},[49] $M_s = 1.1 \times 10^6$ A m^{-1}, $\alpha = 0.03$,[62] and $\theta_{SH} = 0.15$.[63] When a charge current with $j_c = 3.1 \times 10^{13}$ A m^{-2} was applied to the antiferromagnetically coupled system, $\mathbf{m}_1$ and $\mathbf{m}_2$ were first tilted toward the $-x$ direction and then almost aligned antiparallelly along the y axis. Note that $\mathbf{m}_1$ and $\mathbf{m}_2$ acquire the small z component opposite to their initial directions. The turning-off of j_c then resulted in the full switching of the antiferromagnetic order. This switching scheme is consistent with a CoFeB/Ta/CoFeB system.[22] For the case of the ferromagnetically coupled system, on the other hand, $\mathbf{m}_1$ and $\mathbf{m}_2$ first instantaneously exhibited the tilting toward the $-x$ and $+x$ directions, respectively, when the same charge current as before was applied. This was followed by the antiparallel alignment along the y axis, similar to the antiferromagnetically coupled case. Note that $|m_{1z}| > |m_{2z}|$ in this intermediate state ($m_{1z} \leq 0$ and $m_{2z} \geq 0$) because $|\boldsymbol{\sigma}_1| \leq |\boldsymbol{\sigma}_2|$ due to $t_{m1} \geq t_{m2}$ [Inset of the far right figure in Fig. 4(b)]. For the ferromagnetically coupled case, the fact that $\boldsymbol{\sigma}_1$ and $\boldsymbol{\sigma}_2$ are in the opposite directions may appear to be unfavorable, since the spin–orbit torque effect seems to be canceled

between the two layers, as has been discussed above. However, because the interlayer exchange coupling is not very strong, the spin–orbit torque can overcome the former when j_c is sufficiently large and lead temporarily to the "antiferromagnetic" configuration of $\mathbf{m}_1$ and $\mathbf{m}_2$. After turning off j_c, $\mathbf{m}_1$ first started to switch toward the negative z direction, with $\mathbf{m}_2$ dragged by $\mathbf{m}_1$ via the ferromagnetic coupling, to complete the switching into the final ferromagnetically coupled state. Although the antiferromagnetically and the ferromagnetically coupled cases exhibit similar intermediate states during the current application, the switching current density (j_{sw}) can be different for the two cases. Figure 4(c) shows j_{sw} as a function of $|J_{IEC}|$. For $|J_{IEC}| \leq 1.5 \times 10^{-3}$ J m^{-2}, j_{sw} was smaller for the ferromagnetically coupled case. This tendency was widely observed when t_{m2} is varied in the range of 0.3 nm $\leq t_{m2} < 0.8$ nm, as shown in Fig. 4(d). In addition, for the ferromagnetically coupled system, the magnetization switching was observed even when $t_{m2} = 0.792$ nm ($= 0.99 \times t_{m1}$), whereas the switching did not happen when exactly $t_{m1} = t_{m2}$, indicating that the asymmetry in the properties of magnetic layers, such as the difference in the layer thicknesses, is indispensable for the deterministic SOT switching. Based on the macrospin model, therefore, we expect that a ferromagnetically coupled system with relatively low $|J_{IEC}|$ is promising for efficient spin–orbit torque switching.

These calculations also suggest that the formation of the complicated domain structure in Fig. 3(c) may not directly be attributed to the fact that $\boldsymbol{\sigma}_\mu$ lies in the opposite directions in the top and bottom layers. A multiple domain state may be more favored for the ferromagnetically coupled case to lower the magnetostatic energy, accompanied by the domain-wall trapping after the switching. This suggests that the highly efficient switching is expected not only for
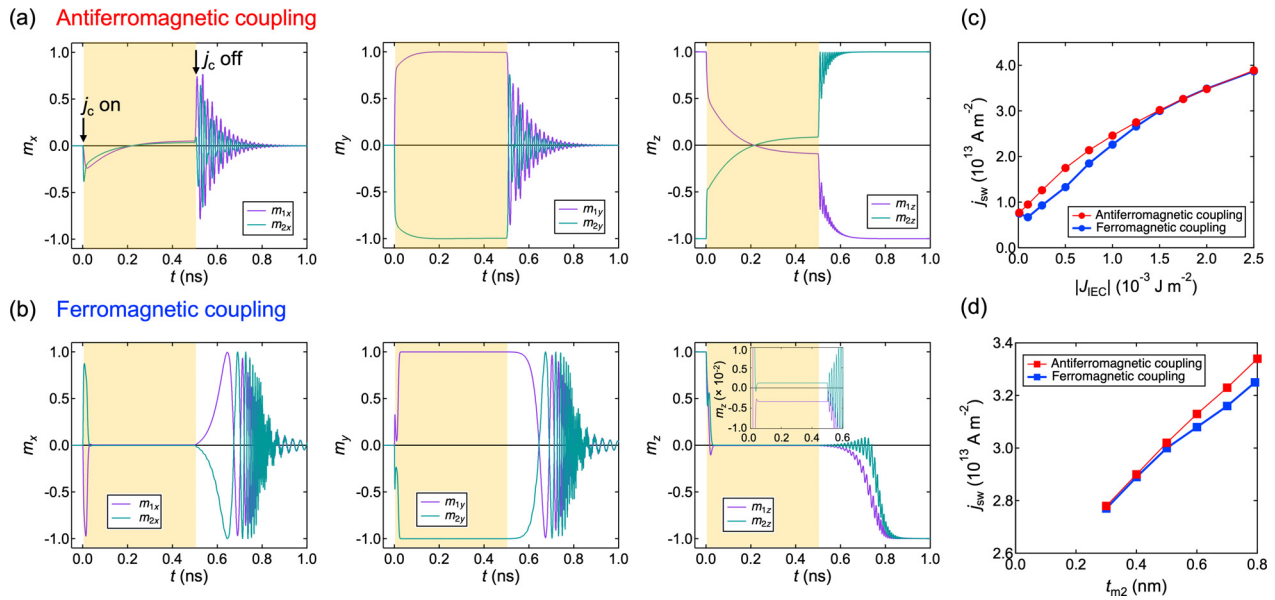

FIG. 4. Numerical calculation of spin–orbit torque switching in a magnetic multilayer with interlayer exchange coupling sandwiched by spin Hall layers. (a) and (b) Switching dynamics for systems with (a) the antiferromagnetic coupling and (b) the ferromagnetic coupling. Left, middle, and right figures show the x, y, and z components of top (m_1) and bottom (m_2) magnetic moments as a function of time, respectively. In the yellow shaded region, $j_c = 3.1 \times 10^{13}$ and 3.15×10^{13} A m^{-2} were applied in (a) and (b), respectively. The enlarged figure of m_z in the intermediate state is shown in the inset of the right figure in (b). Results were calculated using the parameters of $t_{m1} = 0.8$ nm, $t_{m2} = 0.5$ nm, $\mu_0 H_x = -10$ mT, $|J_{IEC}| = 1.5 \times 10^{-3}$ J m^{-2}, $K = 5.7 \times 10^5$ J m^{-3}, $M_s = 1.1 \times 10^6$ A m^{-1}, $\alpha = 0.03$, and $\theta_{SH} = 0.15$. (c) and (d) Switching current density (j_{sw}) as a function of (c) $|J_{IEC}|$ and (d) t_{m2}. In (c), $t_{m1} = 0.8$ and $t_{m2} = 0.5$ nm were used. In (d), t_{m1} was fixed to 0.8 nm.

an antiferromagnetically coupled film but also for a ferromagnetically coupled film if one can fabricate a nanometer-scaled device with its size smaller than the single magnetic domain size.

In summary, we investigated the current-induced magnetization switching in the magnetic multilayer system with interlayer exchange coupling sandwiched by two spin Hall layers of Pt. The domain structures formed during switching varied depending on whether the layers were ferromagnetically coupled or antiferromagnetically coupled. The macrospin calculations for the spin–orbit torque switching revealed that the dual spin–orbit torque from the two Pt layers effectively acts on the two Co layers not only for the antiferromagnetically coupled case but also for the ferromagnetically coupled one. The present results give an understanding of the current-induced magnetization switching mechanism in a magnetic multilayer system and information to design a spintronic device with an efficient magnetization switching.

AUTHOR DECLARATIONS
Conflict of Interest

The authors have no conflicts to disclose.

Author Contributions

Hiroto Masuda: Data curation (equal); Formal analysis (equal); Funding acquisition (equal); Investigation (lead); Writing – original draft (lead). **Koki Takanashi:** Conceptualization (equal); Funding acquisition (equal); Supervision (equal); Writing – review & editing (equal). **Yuta Yamane:** Data curation (equal); Formal analysis (equal); Writing – original draft (supporting). **Takeshi Seki:** Conceptualization (equal); Funding acquisition (equal); Supervision (equal); Writing – review & editing (equal). **Klaus Raab:** Investigation (supporting); Writing – review & editing (equal). **Takaaki Dohi:** Investigation (supporting); Writing – review & editing (equal). **Rajkumar Modak:** Investigation (supporting); Writing – review & editing (equal). **Ken-ichi Uchida:** Funding acquisition (equal); Supervision (equal); Writing – review & editing (equal). **Jun'ichi Ieda:** Supervision (equal); Writing – review & editing (equal). **Mathias Kläui:** Conceptualization (equal); Funding acquisition (equal); Supervision (equal); Writing – review & editing (equal).

DATA AVAILABILITY

The data that support the findings of this study are available from the corresponding authors upon reasonable request.

REFERENCES

[1]A. S. Núñez, R. A. Duine, P. Haney, and A. H. MacDonald, Phys. Rev. B **73**, 214426 (2006).

[2]T. Jungwirth, X. Marti, P. Wadley, and J. Wunderlich, Nat. Nanotechnol. **11**, 231 (2016).

[3]V. Baltz, A. Manchon, M. Tsoi, T. Moriyama, T. Ono, and Y. Tserkovnyak, Rev. Mod. Phys. **90**, 015005 (2018).

[4]L. Néel, Science **174**(4013), 985–992 (1971).

[5]T. Kampfrath, A. Sell, G. Klatt, A. Pashkin, S. Mährlein, T. Dekorsy, M. Wolf, M. Fiebig, A. Leitenstorfer, and R. Huber, Nat. Photonics **5**, 31–34 (2011).

[6]K. Olejník, T. Seifert, Z. Kašpar, V. Novák, P. Wadley, R. P. Campion, M. Baumgartner, P. Gambardella, P. Němec, J. Wunderlich, J. Sinova, P. Kužel, M. Müller, T. Kampfrath, and T. Jungwirth, Sci. Adv. **4**, eaar3566 (2018).

[7]Q. Zhang, Y. Yang, Z. Luo, Y. Xu, R. Nie, X. Zhang, and Y. Wu, Phys. Rev. Appl. **13**, 054016 (2020).

[8]A. Manchon, J. Zelezny, I. M. Miron, T. Jungwirth, J. Sinova, A. Thiaville, K. Garello, and P. Gambardella, Rev. Mod. Phys. **91**, 035004 (2019).

[9]P. Wadley, B. Howells, J. Železný, C. Andrews, V. Hills, R. P. Campion, V. Novák, K. Olejník, F. Maccherozzi, S. S. Dhesi, S. Y. Martin, T. Wagner, J. Wunderlich, F. Freimuth, Y. Mokrousov, J. Kuneš, J. S. Chauhan, M. J. Grzybowski, A. W. Rushforth, K. W. Edmond, B. L. Gallagher, and T. Jungwirth, Science **351**, 587 (2016).

[10]M. J. Grzybowski, P. Wadley, K. W. Edmonds, R. Beardsley, V. Hills, R. P. Campion, B. L. Gallagher, J. S. Chauhan, V. Novak, T. Jungwirth, F. Maccherozzi, and S. S. Dhesi, Phys. Rev. Lett. **118**, 057701 (2017).

[11]T. Moriyama, K. Oda, T. Ohkochi, M. Kimata, and T. Ono, Sci. Rep. **8**, 14167 (2018).

[12]T. Moriyama, W. Zhou, T. Seki, K. Takanashi, and T. Ono, Phys. Rev. Lett. **121**, 167202 (2018).

[13]W. Zhou, T. Seki, T. Kubota, G. E. Bauer, and K. Takanashi, Phys. Rev. Mater. **2**, 094404 (2018).

[14]S. Y. Bodnar, L. Šmejkal, I. Turek, T. Jungwirth, O. Gomonay, J. Sinova, A. A. Sapozhnik, H. J. Elmers, M. Kläui, and M. Jourdan, Nat. Commun. **9**, 348 (2018).

[15]X. Z. Chen, R. Zarzuela, J. Zhang, C. Song, X. F. Zhou, G. Y. Shi, F. Li, H. A. Zhou, W. J. Jiang, F. Pan, and Y. Tserkovnyak, Phys. Rev. Lett. **120**, 207204 (2018).

[16]M. Meinert, D. Graulich, and T. Matalla-Wagner, Phys. Rev. Appl. **9**, 064040 (2018).

[17]A. A. Sapozhnik, M. Filianina, S. Y. Bodnar, A. Lamirand, M. A. Mawass, Y. Skourski, H. J. Elmers, H. Zabel, M. Kläui, and M. Jourdan, Phys. Rev. B **97**, 134429 (2018).

[18]T. Seki, H. Tomita, T. Shinjo, and Y. Suzuki, Appl. Phys. Lett. **97**, 162508 (2010).

[19]S.-H. Yang, K.-S. Ryu, and S. Parkin, Nat. Nanotechnol. **10**, 221 (2015).

[20]A. K. Nandy, N. S. Kiselev, and S. Blügel, Phys. Rev. Lett. **116**, 177202 (2016).

[21]C. Bi, H. Almasi, K. Price, T. Newhouse-Illige, M. Xu, S. R. Allen, X. Fan, and W. Wang, Phys. Rev. B **95**, 104434 (2017).

[22]G. Y. Shi, C. H. Wan, Y. S. Chang, F. Li, X. J. Zhou, P. X. Zhang, J. W. Cai, X. F. Han, F. Pan, and C. Song, Phys. Rev. B **95**, 104435 (2017).

[23]A. Soumyanarayanan, M. Raju, A. L. G. Oyarce, A. K. C. Tan, M.-Y. Im, A. P. Petrović, P. Ho, K. H. Khoo, M. Tran, C. K. Gan, F. Ernult, and C. Panagopoulos, Nat. Mater. **16**, 898 (2017).

[24]R. A. Duine, K.-J. Lee, S. S. P. Parkin, and M. D. Stiles, Nat. Phys. **14**, 217 (2018).

[25]P. X. Zhang, L. Y. Liao, G. Y. Shi, R. Q. Zhang, H. Q. Wu, Y. Y. Wang, F. Pan, and C. Song, Phys. Rev. B **97**, 214403 (2018).

[26]X. Wang, C. Wan, W. Kong, X. Zhang, Y. Xing, C. Fang, B. Tao, W. Yang, L. Huang, H. Wu, M. Irfan, and X. Han, Adv. Mater. **30**, 1801318 (2018).

[27]W. J. Kong, C. H. Wan, B. S. Tao, C. Fang, L. Huang, C. Y. Guo, M. Irfan, and X. F. Han, Appl. Phys. Lett. **113**, 162402 (2018).

[28] X. Li, A. Kang, Z. Liu, and Y. Zhou, Appl. Phys. Lett. **114**, 012403 (2019).

[29] W. J. Kong, C. H. Wan, X. Wang, B. S. Tao, L. Huang, C. Fang, C. Y. Guo, Y. Guang, M. Irfan, and X. F. Han, Nat. Commun. **10**, 233 (2019).

[30] M. Raju, A. Yagil, A. Soumyanarayanan, A. K. C. Tan, A. Almoalem, F. Ma, O. M. Auslaender, and C. Panagopoulos, Nat. Commun. **10**, 696 (2019).

[31] Y. Ishikuro, M. Kawaguchi, N. Kato, Y.-C. Lau, and M. Hayashi, Phys. Rev. B **99**, 134421 (2019).

[32] E. Y. Vedmedenko, P. Riego, J. A. Arregi, and A. Berger, Phys. Rev. Lett. **122**, 257202 (2019).

[33] D.-S. Han, K. Lee, J.-P. Hanke, Y. Mokrousov, K.-W. Kim, W. Yoo, Y. L. W. van Hees, T.-W. Kim, R. Lavrijsen, C.-Y. You, H. J. M. Swagten, M.-H. Jung, and M. Kläui, Nat. Mater. **18**, 703 (2019).

[34] A. Fernández-Pacheco, E. Vedmedenko, D. Petit, and R. P. Cowburn, Nat. Mater. **18**, 679 (2019).

[35] M. Schmitt, P. Moras, G. Bihlmayer, R. Cotsakis, M. Vogt, J. Kemmer, A. Belabbes, P. M. Sheverdyaeva, A. K. Kundu, C. Carbone, S. Blügel, and M. Bode, Nat. Commun. **10**, 2610 (2019).

[36] Y.-C. Lau, Z. Chi, T. Taniguchi, M. Kawaguchi, G. Shibata, N. Kawamura, M. Suzuki, S. Fukami, A. Fujimori, H. Ohno, and M. Hayashi, Phys. Rev. Mater. **3**, 104419 (2019).

[37] T. Dohi, S. DuttaGupta, S. Fukami, and H. Ohno, Nat. Commun. **10**, 5153 (2019).

[38] Y. Ishikuro, M. Kawaguchi, T. Taniguchi, and M. Hayashi, Phys. Rev. B **101**, 014404 (2020).

[39] K. Wang, L. Qian, S.-C. Ying, and G. Xiao, Commun. Phys. **4**, 10 (2021).

[40] H. Masuda, T. Seki, Y.-C. Lau, T. Kubota, and K. Takanashi, Phys. Rev. B **101**, 224413 (2020).

[41] L. Zhu, X. Xu, M. Wang, K. Meng, Y. Wu, J. Chen, J. Miao, and Y. Jianga, Appl. Phys. Lett. **117**, 112401 (2020).

[42] Q. Ma, Y. Li, Y.-S. Choi, W.-C. Chen, S. J. Han, and C. L. Chien, Appl. Phys. Lett. **117**, 172403 (2020).

[43] S. D. Pollard, J. A. Garlow, K.-W. Kim, S. Cheng, K. Cai, Y. Zhu, and H. Yang, Phys. Rev. Lett. **125**, 227203 (2020).

[44] R. Q. Zhang, G. Y. Shi, J. Su, Y. X. Shang, J. W. Cai, L. Y. Liao, F. Pan, and C. Song, Appl. Phys. Lett. **117**, 212403 (2020).

[45] M. C. H. de Jong, C. O. Avci, A. Hrabec, and P. Gambardella, Phys. Rev. B **102**, 174433 (2020).

[46] X. Xie, X. Zhao, Y. Dong, X. Qu, K. Zheng, X. Han, X. Han, Y. Fan, L. Bai, Y. Chen, Y. Dai, Y. Tian, and S. Yan, Nat. Commun. **12**, 2473 (2021).

[47] C. O. Avci, C.-H. Lambert, G. Sala, and P. Gambardella, Phys. Rev. Lett. **127**, 167202 (2021).

[48] Y. Saito, S. Ikeda, and T. Endoh, Phys. Rev. B **105**, 054421 (2022).

[49] H. Masuda, T. Seki, Y. Yamane, R. Modak, K. Uchida, J. Ieda, Y.-C. Lau, S. Fukami, and K. Takanashi, Phys. Rev. Appl. **17**, 054036 (2022).

[50] R. Macêdo, A. S. Kudinoor, K. L. Livesey, and R. E. Camley, Adv. Electron. Mater. **8**, 2100435 (2022).

[51] S. G. Jeong, J. Kim, A. Seo, S. Park, H. Y. Jeong, Y.-M. Kim, V. Lauter, T. Egami, J. H. Han, and W. S. Choi, Sci. Adv. **8**, eabm4005 (2022).

[52] G. Binasch, P. Grünberg, F. Saurenbach, and W. Zinn, Phys. Rev. B **39**, 4828(R) (1989).

[53] S. S. P. Parkin, Phys. Rev. Lett. **67**, 3598 (1991).

[54] S. Woo, M. Mann, A. J. Tan, L. Caretta, and G. S. D. Beach, Appl. Phys. Lett. **105**, 212404 (2014).

[55] J. Yu, X. Qiu, W. Legrand, and H. Yang, Appl. Phys. Lett. **109**, 042403 (2016).

[56] R. Wang, Z. Xiao, H. Liu, Z. Quan, X. Zhang, M. Wang, M. Wu, and X. Xu, Appl. Phys. Lett. **114**, 042404 (2019).

[57] Y. Wu, X. Zeng, Y. Guo, Q. Jia, B. Wang, and J. Cao, Appl. Phys. Lett. **118**, 022401 (2021).

[58] Y. Cao, X. N. Bian, Z. Yan, L. Xi, N. Lei, L. Qiao, M. S. Si, J. W. Cao, D. Z. Yang, and D. S. Xue, Appl. Phys. Lett. **119**, 012401 (2021).

[59] L. Zhu, D. C. Ralph, and R. A. Buhrman, Appl. Phys. Rev. **8**, 031308 (2021).

[60] A. Himeno, S. Kasai, and T. Ono, Appl. Phys. Lett. **87**, 243108 (2005).

[61] C. Moreau-Luchaire, C. Moutafis, N. Reyren, J. Sampaio, C. A. F. Vaz, N. Van Horne, K. Bouzehouane, K. Garcia, C. Deranlot, P. Warnicke, P. Wohlhüter, J.-M. George, M. Weigand, J. Raabe, V. Cros, and A. Fert, Nat. Nanotechnol. **11**, 444–448 (2016).

[62] N. Fujita, N. Inaba, F. Kirino, S. Igarashi, K. Koike, and H. Kato, J. Magn. Magn. Mater. **320**, 3019 (2008).

[63] M.-H. Nguyen, D. C. Ralph, and R. A. Buhrman, Phys. Rev. Lett. **116**, 126601 (2016).